Journal of Environmental Chemical Engineering 10 (2022) 108373

Contents lists available at ScienceDirect

Journal of Environmental Chemical Engineering

journal homepage: www.elsevier.com/locate/jece

Rapid biological reduction of graphene oxide: Impact on methane production and micropollutant transformation

Michele Ponzelli [a,b,c], Soraya Zahedi [d], Konrad Koch [c], Jörg E. Drewes [c], Jelena Radjenovic [a,e,*]

[a] Catalan Institute for Water Research (ICRA), Emili Grahit 101, 17003 Girona, Spain
[b] University of Girona, 17003 Girona, Spain
[c] Chair of Urban Water Systems Engineering, Technical University of Munich, Am Coulombwall 3, 85748 Garching, Germany
[d] Instituto de la Grasa, Spanish National Research Council (CSIC), Campus Universitario Pablo de Olavide, Ed. 46, Ctra. De Utera, 41013 Seville, Spain
[e] Catalan Institution for Research and Advanced Studies (ICREA), Passeig Lluís Companys 23, 08010 Barcelona, Spain

ARTICLE INFO

Editor: Despo Kassinos

Keywords:
Bioreduced graphene oxide
Microbial reduction
Organic micropollutants
Biogas production
Anaerobic digestion

ABSTRACT

This study investigates the impact of graphene oxide (GO) addition to anaerobic sludge and the formation of biologically reduced GO (bioRGO) on both the anaerobic transformation of organic contaminants and the corresponding biogas production. A hydrogel-like material of anaerobic digestate and bioRGO was formed on the first day after GO addition. Raman spectroscopy showed an increase in the I_D/I_G ratio from 0.74 to 1.01, confirming the reduction of GO due to anaerobic respiration. The anaerobic removal of model antibiotics sulfamethoxazole and trimethoprim was unaffected by the GO addition. Yet formation of bioRGO inhibited the formation of the identified transformation products (TPs) of sulfamethoxazole, TP253 and TP257. Furthermore, the formation of TP253 and TP257 biotransformation products of sulfamethoxazole in sterilized sludge confirmed that their removal was likely achieved via intracellular enzymes that had enough thermal stability to remain active after the sterilization. For trimethoprim, no transformation products could be detected using the employed analytical method. The production of methane was generally inhibited up to 18% due to the presence of high GO levels (>100 mg/L) (288 vs. 353 mL CH_4/g VS).

1. Introduction

Climate change and population growth are putting increased pressure on the implementation of technologies that address the water-energy nexus and enable water, energy, and cost recovery. Conventional wastewater treatment plants (WWTPs) employing aerobic activated sludge processes might become obsolete due to their high energy demand, large amounts of sludge produced, and loss of nutrients [1]. Novel anaerobic wastewater treatment technologies can offset the energy and greenhouse gas costs of the activated sludge process and even become net energy producers [2]. They offer an opportunity to recover valuable soil amendment, drastically reduce the quantity of the produced sludge, and can facilitate the implementation of decentralized wastewater treatment [3]. Nevertheless, anaerobic processes suffer from long start-up times, low removal rates of organic pollutants, and susceptibility to disruptions by the organic overload [4].

The addition of low-cost conductive materials (e.g., granular activated carbon, biochar, magnetite, graphene-like materials) to anaerobic systems is an attractive strategy to promote the interspecies electron transfer (IET) between fermentative bacteria and the methanogens, and thus enhance the degradation of organics and methane production [5,6]. Microbial reduction of graphene oxide (GO) to bio-reduced graphene oxide (bioRGO) has drawn significant interest due to the changes it induces in the morphology and behavior of the anaerobic consortia [7,8], with some studies reporting the self-aggregation of the bacteria in a hydrogel-like structure [8,9]. Microbial reduction of GO can be achieved by single bacterial strains, such as *Escherichia coli* [10], *Shewanella* [11], as well as by mixed microbial communities [12] and anammox bacteria [13] too. However, working with laboratory-adapted sludge may not represent the anaerobic culture present in the full-scale digestor. In order to investigate the impact of GO on the behavior of the real culture of the anaerobic digester, experiments in this study were conducted using freshly sampled sludge.

Regarding the impact of the bioRGO on methanogenesis, several studies reported an inhibiting effect at high GO concentrations (i.e., 500–1440 mg/L) [14,15], likely due to the consumption of the electrons

* Corresponding author at: Catalan Institute for Water Research (ICRA), Emili Grahit 101, 17003 Girona, Spain.
E-mail address: jradjenovic@icra.cat (J. Radjenovic).

https://doi.org/10.1016/j.jece.2022.108373
Received 5 May 2022; Received in revised form 27 June 2022; Accepted 30 July 2022
Available online 2 August 2022

by GO reduction instead of methane formation [16]. Yet, graphene material amended to anaerobic digestate leads to higher methane production yields and rates, with up to 51.4% more when a concentration of 120 mg/L is applied [17]. It is unclear whether GO exerts toxic effects on the microorganisms. For example, Liu et al. [18] observed loss of *E. coli* viability with GO addition (40 mg/L). On the contrary, Guo et al. [19] reported a significant enhancement in *E. coli* and *Staphylococcus aureus* cell growth and biofilm formation with the addition of GO, even up to a concentration of 500 mg/L. Perreault et al. [20] demonstrated that the antibacterial activity of GO is size-dependent, with smaller GO sheets having a higher density of defects inducing higher oxidative stress to the cells.

In addition, bioRGO was observed to enhance the biotransformation and reduction of a range of organic and inorganic contaminants, such as dyes [9,21], nitroaromatics [21–23] and halogenated aromatics [23, 24]. However, the fate of trimethoprim (TMP) and sulfamethoxazole (SMX), two antibiotics commonly used in human and veterinary medicine, in the anaerobic digestion with bioRGO was not explored yet. They are typically administered together and were selected due to their inclusion in the third Watch List under the EU Water Framework Directive (Directive 2008/105/EC) [25]. Moreover, high concentration levels of SMX (above 5 mg/L) are known to negatively affect the anaerobic microbial population, while 0.5–5 mg/L level might positively affect the anaerobic digestion performance [26–28]. In this study, environmentally relevant concentrations were selected for both SMX and TMP (0.2 μM, i.e., 61 and 70 μg/L, respectively) [29,30].

In this study, we investigated the impact of GO addition in the range from 10 to 500 mg/L of GO (i.e., 0.9–46.8 mg GO per g of volatile solids, VS) on methane production and biotransformation of TMP and SMX. Moreover, the microbial reduction of GO to bioRGO and changes in the sludge morphology were characterized using Raman spectroscopy, optical microscopy, and particle size analysis. The removal of contaminants by abiotic effects (e.g., adsorption onto the GO and the sludge matrix) was checked by controlling with an aqueous GO solution and sterilized sludge. Although sludge sterilization may change sludge characteristics, it is still used to allow an indication of contaminant adsorption. To gain insight into the biotransformation pathway of the selected contaminants, several transformation products (TPs) were tentatively identified.

The hypothesis tested in this study is whether the presence of bioRGO can significantly improve the biotransformation of the two selected antibiotics and the methane production compared to a control. Compared to previous approaches, this study followed the biochemical methane potential (BMP) guidelines set by Holliger et al. [31], which include the use of a standard substrate and specific termination criteria. Additionally, the main novelty of this work is the investigation of the GO impact on the anaerobic biotransformation of antibiotics, and their TPs behavior, which is relevant for novel anaerobic wastewater treatment processes, such as anaerobic membrane bioreactor (AnMBR), up-flow anaerobic sludge blanket (UASB), anaerobic biofilm reactors, and similar reactor configurations.

2. Materials and methods

2.1. Materials and chemicals

The GO was provided from Graphenea (San Sebastián, Spain) as a 4 g/L aqueous dispersion, with a flake size < 10 μm. Analytical standards for SMX and TMP and microcrystalline cellulose (MCC) were purchased from Merck (Madrid, Spain). Isotopically labeled standards SMX-d4 and TMP-d3 were purchased from LGC Standards (Barcelona, Spain). All reagents used for sample preparation and analysis were of analytical grade.

2.2. Experimental setup

The inoculum used in the experiments was collected from the anaerobic digester of the WWTP in Girona, Spain, working at mesophilic temperature (35 °C) and treating primary and secondary sludge. The content of total solids (TS) and volatile solids (VS) of the inoculum was 1.9% and 1.2%, respectively. The experiments were conducted with MCC as substrate. As recommended when using MCC, the inoculum substrate ratio (ISR) was set to 2 based on VS [31].

To study the impact of the GO and the presence of contaminants on the formation of methane, BMP tests were conducted with inoculum, substrate (MCC), 0, 10, 100, and 500 mg/L of GO, and with and without the addition of antibiotics. BMP tests were performed in triplicate using sealed 240 mL bottles with 150 mL of working volume. The sludge characteristics are summarized in Table S1, Supporting material. GO, MCC, and antibiotics were added to the inoculum prior to incubation, and pH control was not controlled. Before sealing the BMP bottles, the headspace was flushed with nitrogen gas for one minute to guarantee anaerobic conditions. All the bottles were stored in a temperature-controlled incubator at 35 °C. All bottles were placed on an orbital shaker at 50 rpm to ensure sufficient mixing. Accumulated methane was determined by measuring the biogas production and methane content once a day for the first 10 days and every 3–4 days thereafter. Biogas volume was measured with a pressure sensor (PM7097, ifm electronic, Barcelona, Spain) at the bottle headspace. After each measurement, the bottle headspace was vented to ambient pressure. CH_4 concentration was measured using an infrared sensor (GIR-3000, Gastron Co., Gyeonggi-do, Korea). According to the previously published guidelines, the results were normalized to temperature, pressure, and water vapor partial pressure [32]. Cumulative gas productions were calculated by subtracting the endogenous methane production obtained from blanks, i.e., assays containing only inoculum. Relative standard error bars based on the triplicate measurements were calculated according to [33].

To evaluate the impact of the GO addition on the removal of target antibiotics, experiments were performed using an additional set of BMP bottles. Such extra bottles were not included in the determination of methane production. SMX and TMP were added simultaneously at the initial concentration of 0.24 μM each to have amounts comparable to environmental concentrations observed in sewage sludge [29,30]. Samples (~2 mL) were withdrawn at designated time intervals. After sampling, the bottles were purged with a gentle nitrogen stream to remove the oxygen from the headspace. Prior to analysis, the samples were centrifuged and filtered using a 0.2 μm hydrophilic polytetrafluoroethylene (PTFE) membrane filter (Millex, Merck, Madrid, Spain). To evaluate the adsorption of the contaminants on the GO, experiments were performed using 500 mg/L of GO solution in milli-Q water. Additional experiments with the sludge sterilized by autoclaving at 120 °C for 20 min were performed to evaluate the adsorption of the antibiotics on sterilized sludge. Table 1 summarizes all the different experimental settings investigated. To identify possible TPs formed during anaerobic biotransformation, experiments were performed by adding SMX and TMP separately at higher initial concentrations (i.e., 40 μM) to anaerobic sludge and varying concentrations of GO (i.e., 0, and 500 mg/L). The formation of the identified TPs was later confirmed in the experiments conducted at lower initial concentration of antibiotics (i.e., 0.24 μM).

2.3. Analytical methods

The target antibiotics were analyzed in the selected reaction monitoring (SRM) mode using a hybrid triple quadrupole-linear ion trap mass spectrometer (5500 QTRAP, Applied Biosystems, Waltham, USA) with a Turbo Ion Spray source, coupled to a liquid chromatograph (Waters Acquity Ultra-Performance™, Waters Corporation, Milford, USA), according to the previously published method [29]. To correct the matrix interferences, the quantification was performed using isotopically

Table 1
Summary of the different experimental settings (n = 3, †: n = 6). The following abbreviations are used: microcrystalline cellulose (MCC); sterilized sludge (SS); control assays without antibiotics (CTRL); assays with antibiotics (ANT).

Inoculum	Substrate	Antibiotics	GO concentration (mg/L) and experiment name			
			0	10	100	500
Absent	None	0.24 μM	–	–	–	500
Present	None	None	Blank	–	–	–
		0.24 μM	SS	–	–	–
	MCC	None	CTRL	CTRL10	CTRL100	CTRL500
		0.24 μM	ANT†	ANT10†	ANT100†	ANT500†

labeled standards (i.e., SMX-d4 and TMP-d3). Tentative identification of the TPs of antibiotics was performed by full-scan mode of analysis, isolation of the protonated molecular ions, collision induced dissociation (CID) MS^2 experiments in the positive electrospray mode, and mass spectral comparison with the parent compound, as well as with the literature data.

According to the Standard Methods, TS and VS were analyzed [34]. Total and soluble (filtered at 0.45 μm) chemical oxygen demand (COD) were analyzed using LCK114 test kits (Hach Lange, Germany). Ammonium (NH_4^+) concentration was measured via ion chromatography (IC) (Dionex ICS-5000, Thermo Fisher Scientific, Waltham, USA), and total alkalinity concentration was measured via titration (855 Robotic Titrosampler, Metrohm, Filderstadt, Germany). pH and conductivity were measured using a pH meter (GLP21 Crison, Hach Lange, Barcelona, Spain) and a conductometer (GLP 31 + Crison, Hach Lange, Barcelona, Spain). The size of the sludge flocs was evaluated using an inverted optical microscope (Eclipse Ti-S, Tokyo, Nikon) and a laser diffraction particle size analyzer (LS 13 320, Beckman Coulter Inc., Brea, USA). A dispersive spectrometer (Jobin-Yvon LabRam HR 800, Horiba, Madrid, Spain) coupled with an optical microscope (Olympus BXFM, Olympus Iberia, Barcelona, Spain) was used for Raman characterization. The CCD detector was cooled at − 64 °C, and a 532 nm laser line was used with a dispersive grating of 600 lines mm^{-1} and a laser power at sample of 0.5 mW. The Raman spectroscopy analysis was performed for the sludge inoculum with 500 mg/L of added GO on days 0, 1 and 15, to verify the formation of the bioRGO. Moreover, Raman spectroscopy was also performed on the sterilized sludge inoculum with 100 mg/L of added GO to verify if any formation of bioRGO occurs without the viable microbial community. To investigate the redox activity of the sludge supernatant, cyclic voltammetry (CV) experiments were performed with the fresh anaerobic inoculum and inoculum on day 15 of the experiments conducted in the presence of 500 mg/L of GO, using a three-electrode set-up, with glassy carbon as the working electrode, platinum electrode as the counter electrode, and 3 M Ag/AgCl reference electrode (BASi, Lafayette, USA). The CV was performed using a 5 mV/s scan rate ranging from − 1.5 to + 1.5 V vs. Ag/AgCl, using a BioLogic multi-channel potentiostat/galvanostat VMP-300.

2.4. Gompertz model and statistical analysis

A modified Gompertz kinetic model was used to get more information on the methanogenic process, allowing the determination of the maximum methane production rate (R_{MAX}) and the lag-phase length (λ) [35].

$$B(t) = B_\infty \cdot e^{-e^{\left(\frac{R_{MAX}\cdot e}{B_0}(\lambda - t)+1\right)}}$$

Such parameters were calculated through iteration using the MS Excel solver function. The objective function was the relative standard square error (RSS), set as minimum. The relative root means square error (rRMSE) and the coefficient of determination R^2 were used to assess the model's fitness and efficiency [36]. Initial iteration values of infinite methane production (B_∞), R_{MAX}, and λ are set at 1. All variables are constrained to non-negative values (≥ 0), and ultimate BMP (B_∞) is constrained to values less than or equal to 414 mL CH_4/g VS. This upper limit represented the maximum (100%) theoretical BMP for MCC ($(C_6H_{10}O_5)_n$), as provided by the *Online Biogas App* (OBA) [37].

Moreover, two-way analyses of variance (ANOVA) are carried out using Origin2021 software (OriginLab Corporation, Northampton, Massachusetts, US) to evaluate statistical differences among the different experimental conditions, considering significant values of $p < 0.05$.

3. Results and discussion

3.1. Characterization of the bioRGO-amended inoculum

Raman spectroscopy measurements confirmed the biological reduction of GO to bioRGO (Table 2). The level of defects in the initial GO and bioRGO was calculated by measuring the intensity ratio of the D peak at 1347 cm^{-1} (I_D) and the G peak at 1581 cm^{-1} (I_G) obtained using Raman spectroscopy (Fig. 1). The I_D/I_G ratio of zero represents no defects, and a higher ratio means higher content of graphene defects. At the beginning of the experiments, the measured I_D/I_G ratio was 0.74 for the initial anaerobic sludge (AS) with added GO. This ratio increased to 1.01 after 1 day of anaerobic incubation, evidencing a rapid microbial reduction of GO to bioRGO and the formation of defects (Table 2). Similar rapid (< 1 day) reduction was reported previously for pure anaerobic cultures amended with GO like *Shewanella* [38], *E. Coli* [39], *Geobacter sulfurreducens* [40], and others [8,9]. However, only Shaw et al. [13] demonstrated biological reduction from the mixed microbial community, but only after 9 days. Moreover, the I_D/I_G ratio decreased to 0.82 on day 15, indicating further changes in the structure of bioRGO. This may be due to an increased ordering of the sp^2 bonded graphitic domains and reduction of oxygen moieties in the graphitic lattice [41,42]. The same sample presents a peak at the D+D′ (around 2900 cm^{-1}), which also confirmed the formation of RGO [13]. In the experiments with the sterilized sludge (SS) and added 100 mg/L of GO, the I_D/I_G ratio remained relatively unchanged, with I_D/I_G ratios of 0.71 and 0.68 on day 1 and day 15, respectively (Fig. 1**b**, Table 2). This result confirms that the microbial reduction of GO was occurring only in the presence of a biologically-active microbial community.

The particle size analysis of AS with 500 mg/L of GO added showed a progressive increase in the floc size, with the measured mean particle diameters of 75 μm and 195 μm on day 1 and 15 of the experiment, respectively (Fig. 2**a**). On the other hand, control samples (i.e., sludge without GO) showed no change in particle size, obtaining 51.3 and 57.5 μm on days 1 and 15. In addition, for samples with GO, a right shift of the differential volume peak towards higher particle diameters was noted, and for the sample on day 15, the volumetric distribution curve showed a higher percentage (≥25%) of particles with an estimated diameter > 200 μm. However, it is important to note that this size distribution measurement of the suspended particles was based on the principles of light scattering and gives only an indicative size for non-spherical particles, such as sludge flocs, as their irregular size and shape makes them difficult to measure and quantify. From the optical microscope images of the sludge (Fig. S1), it was evident that the

Table 2
Peak intensities and relative I_D/I_G ratios for GO-amended anaerobic sludge (AS) and sterilized sludge (SS) samples.

		AS+GO			SS+GO	
	I_D (1347 cm^{-1})	I_G (1581 cm^{-1})	I_D/I_G	I_D (1347 cm^{-1})	I_G (1581 cm^{-1})	I_D/I_G
Day 0	98.89	134.06	0.74	98.89	134.06	0.74
Day 1	130.29	129.40	1.01	94.56	133.81	0.71
Day 15	109.68	132.97	0.82	91.21	134.21	0.68

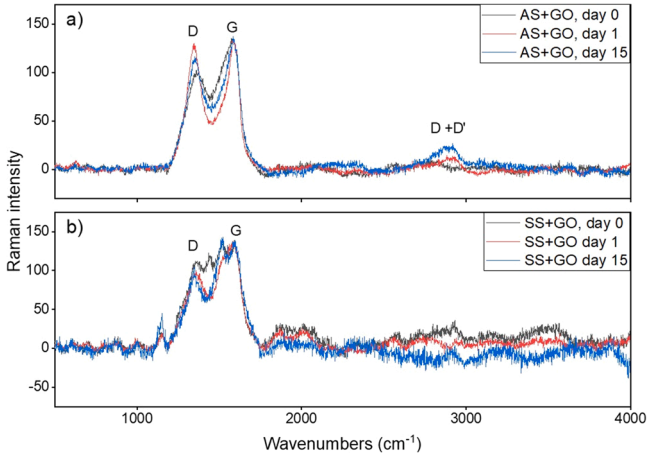

Fig. 1. Raman spectra of **a)** anaerobic sludge (AS) with graphene oxide (GO) added on day 0, 1, and 15, and **b)** sterilized sludge (SS) amended with GO on day 0, 1 and 15.

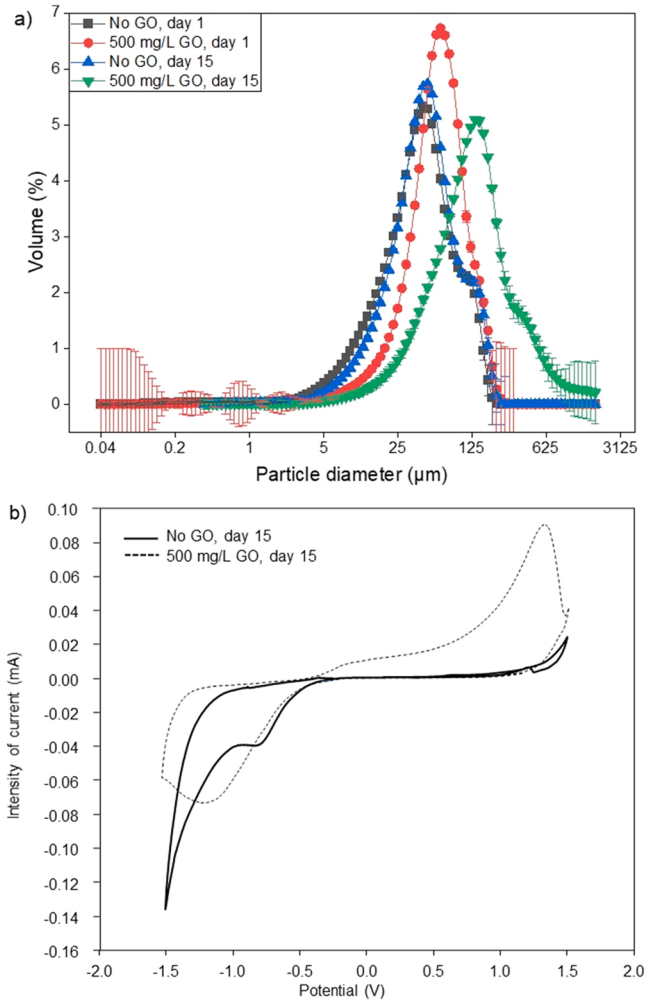

Fig. 2. a) Log scale of the particle size distribution for the sample with and without added GO at 500 mg/L on day 1 and day 15. The results are presented as mean values of three replicates with their standard deviations, and **b)** Cyclic voltammetry (CV) of anaerobic sludge with and without 500 mg/L of GO on day 15.

formation of bioRGO led to a significant increase in the sludge floc size. For example, the observed floc diameters of 63–131 μm for anaerobic inoculum were increased with 500 mg/L of GO to 325–689 μm after 1 day of anaerobic treatment and up to 1223 μm after 15 days.

Fig. 2**b** illustrates the cyclic voltammetry (CV) measurements obtained for the anaerobic sludge inoculum samples on day 15 of the BMP tests conducted in the absence and presence of 500 mg/L of GO. The positive scan of the supernatant of the anaerobic inoculum did not show any anodic peaks, whereas in the reverse scan there was a reduction peak at − 0.6 V vs. the Standard Hydrogen Electrode (SHE). In the supernatant from the sample with the bioRGO, two peaks appeared in the CV scan, at 1.5 V and − 1 V/SHE, indicating the presence of redox-active compounds in the supernatant of bioRGO-modified sludge. In addition, the larger area of the CV from the bioRGO assay indicates a larger capacitance of this supernatant compared with the unmodified anaerobic inoculum. This can be explained by the higher content of the capacitive material (e.g., electron shuttles) formed in the bioRGO inoculum, likely due to the enhanced activity exoelectrogens [43]. Increased capacitance with bioRGO was previously observed in the CV measurements obtained from the GO-amended *Geobacter sp.* strain R4 [8].

It was demonstrated that the added GO was already bioreduced by the mixed anaerobic culture within a few days. This bioRGO is highly redox-active and tends to form a hydrogel with a larger floc size. Whether the presence of the bioRGO impacts the overall anaerobic digestion process is discussed in the next section.

3.2. Impact of bioRGO on the biogas production

The specific methane production (SMP) curves from each condition investigated are depicted in Fig. 3. Dixon's test revealed the presence of two outliers with a significance level ($p < 0.05$) for both the conditions with the addition of 100 mg/L of GO, with and without antibiotics (Fig. S2). These two were excluded from further data analysis. For all the conditions tested, an initial lag phase of about two days was noticed, which is quite common when microcrystalline cellulose is used as a substrate [44]. The two straight dotted lines of Fig. 3 represent the minimum and maximum BMP of cellulose, i.e., 340–395 mL CH_4/g VS, which should be achieved to validate the test results [45]. In the experiments without added GO, the SMP reached 354 ± 31 and 373 ± 26 mL CH_4/g VS in the absence and presence of antibiotics, respectively. Thus, the addition of SMX and TMP at low initial concentrations of 0.24 μM did not significantly influence biogas production. The addition of GO at lower concentrations (10 mg/L, i.e., 0.9 mg GO/g VS) did not impact the SMP in the absence of antibiotics by 5%, but led to a decreased performance when antibiotics were present (i.e., 15% inhibition) (Fig. 4). The presence of 100 mg/L of GO (9.4 mg GO/g VS) inhibited the anaerobic digestion process in both the absence (9% inhibition) and presence of antibiotics (21% inhibition). Thus, although

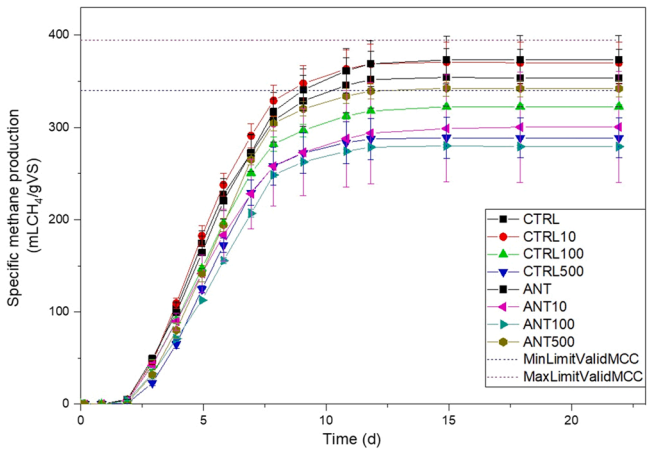

Fig. 3. Specific methane production (SMP) of AS with different GO dosages, with and without added antibiotics (at 0.24 μM initial concentration). See Table 1 for details. The results are presented as mean values of triplicate measurements (where applicable) with standard deviations. The straight dotted lines represent the minimum and maximum validation BMP of cellulose, i.e., 340 and 395 mL CH_4/g VS.

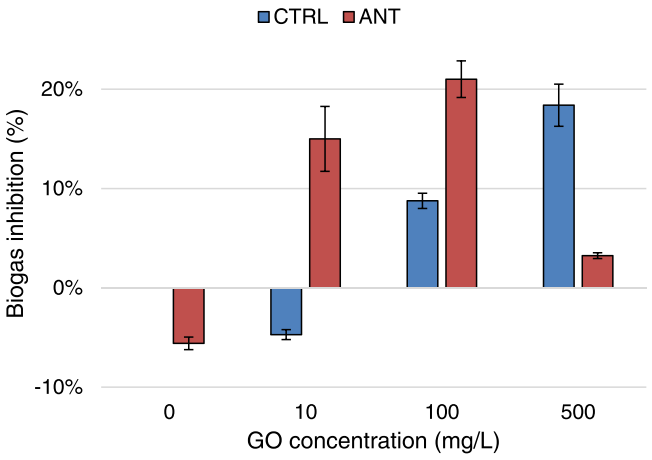

Fig. 4. Biogas inhibition for the different GO levels without and with antibiotics (CTRL and ANT, respectively), compared to the control assay with no GO and antibiotics. The results are presented as mean values of triplicate measurements (where applicable) with standard deviations.

the addition of antibiotics did not impact methane production, their simultaneous presence with the GO led to a more pronounced inhibiting effect within the range of 10–100 mg/L GO. In the experiments with 500 mg/L of GO (46.8 mg GO/g VS), biogas production decreased by 18% without antibiotics. However, in the presence of antibiotics (ANT500), the inhibition at 500 mg/L GO was only 3%, resulting in an overall higher amount of methane formed (i.e., 342 mL CH_4/g VS) compared to CTRL500 (i.e., 289 mL CH_4/g VS), which had no antibiotics. Thus, while GO addition inhibits biogas formation linearly, similar to previously reported findings [14], exposure of sludge to low μM concentrations of antibiotics impacts the response of the microbial community to the addition of an external electron acceptor (i.e., GO). In the presence of antibiotics, the highest inhibition of the process by GO addition was observed at 100 mg/L of GO. The literature previously reported a bell-shaped impact of GO on biogas production and microbial activity [15,46]. For example, Wang et al. reported a bell-shaped impact of GO addition on the activity and extracellular polymeric substances (EPS) production of annamox bacteria [46].

Therefore, the result of the BMP tests demonstrates that the GO addition impacts the performance of anaerobic sludge. As illustrated in Fig. 4, increasing the GO concentrations led to increased biogas inhibition. On the other hand, when antibiotics were amended, the biogas inhibition behaved in a bell-shaped way. Hence, it is unclear which level of GO concentration might not have an inhibiting impact on the anaerobic activity and if BMP tests are the proper method to comprehensively elucidate its impact on anaerobic sludge. Furthermore, two-way ANOVA analysis did not reveal any significant ($p < 0.05$) differences in biogas production between the assays containing antibiotics and the ones without.

As already mentioned, the bioreduction of GO might indeed limit the number of electrons otherwise available for methane production during the first feeding phase [16]. Once the bioreduction GO is completed, it is hypothesized that GO might not consume more electrons thereafter. Continuously or with multiple refeed set-up, it might be helpful to determine the real impact of GO reduction on the methane yield after the initial phase.

3.2.1. *Gompertz model and statistical analysis*

As it can be inferred from Fig. S3, the experimental values of the methane production perfectly fit the Gompertz model achieving an R^2 of 1.0 ± 0.0 and an rRMSE of 0.0% for all tested assays (Table S2).

Moreover, the two-way ANOVA analysis revealed no significant ($p < 0.05$) differences for B_∞ and R_{MAX} across the different experimental conditions. However, further statistical tests on the lag-phase length λ revealed a significant difference ($p < 0.05$) between conditions containing 500 mg/L vs. 0 mg/L of GO and 500 mg/L vs. 10 mg/L of GO. Therefore, it can be suggested that high GO concentrations (500 mg/L) could play a major role in inducing significant delays in biogas production. Fig. 5.

3.3. *Impact of bioRGO on the removal of organic pollutants*

Fig. 6 shows the observed removals of SMX and TMP in the presence of different GO concentrations (0, 10, 100, and 500 mg/L) and the control experiments conducted with the sterilized sludge and only GO solution (500 mg/L) to understand their removal due to adsorption onto sludge and GO nanosheets, respectively. In the control experiments with sterilized sludge, both SMX (Fig. 6**a**) and TMP (Fig. 6**c**) were rapidly removed in the first few days. In the case of SMX, complete removal was obtained already in the first 24 h, similar to the experiments conducted with biologically-active anaerobic sludge (Fig. 6**b**). Even though the sludge underwent sterilization procedures (i.e., 120 °C, 20 min), the removal of SMX in the experiments with sterilized sludge was likely due

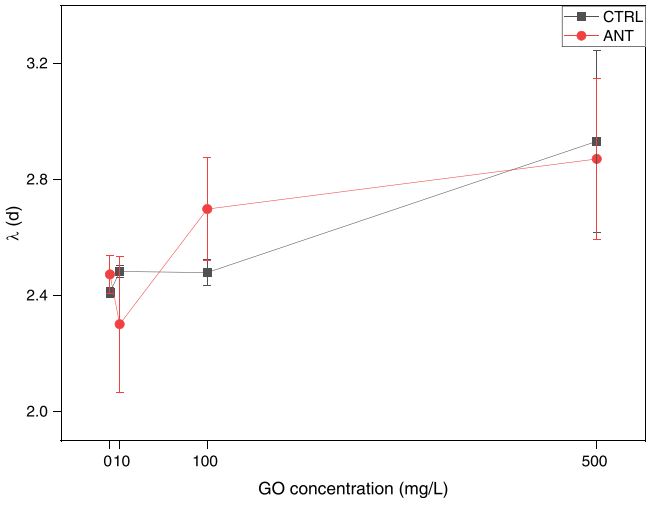

Fig. 5. Lag-phase length for condition without (CTRL) and with antibiotics (ANT) at four GO levels (i.e., 0, 10, 100, 500 mg/L). Error bars represent standard deviations (n = 3).

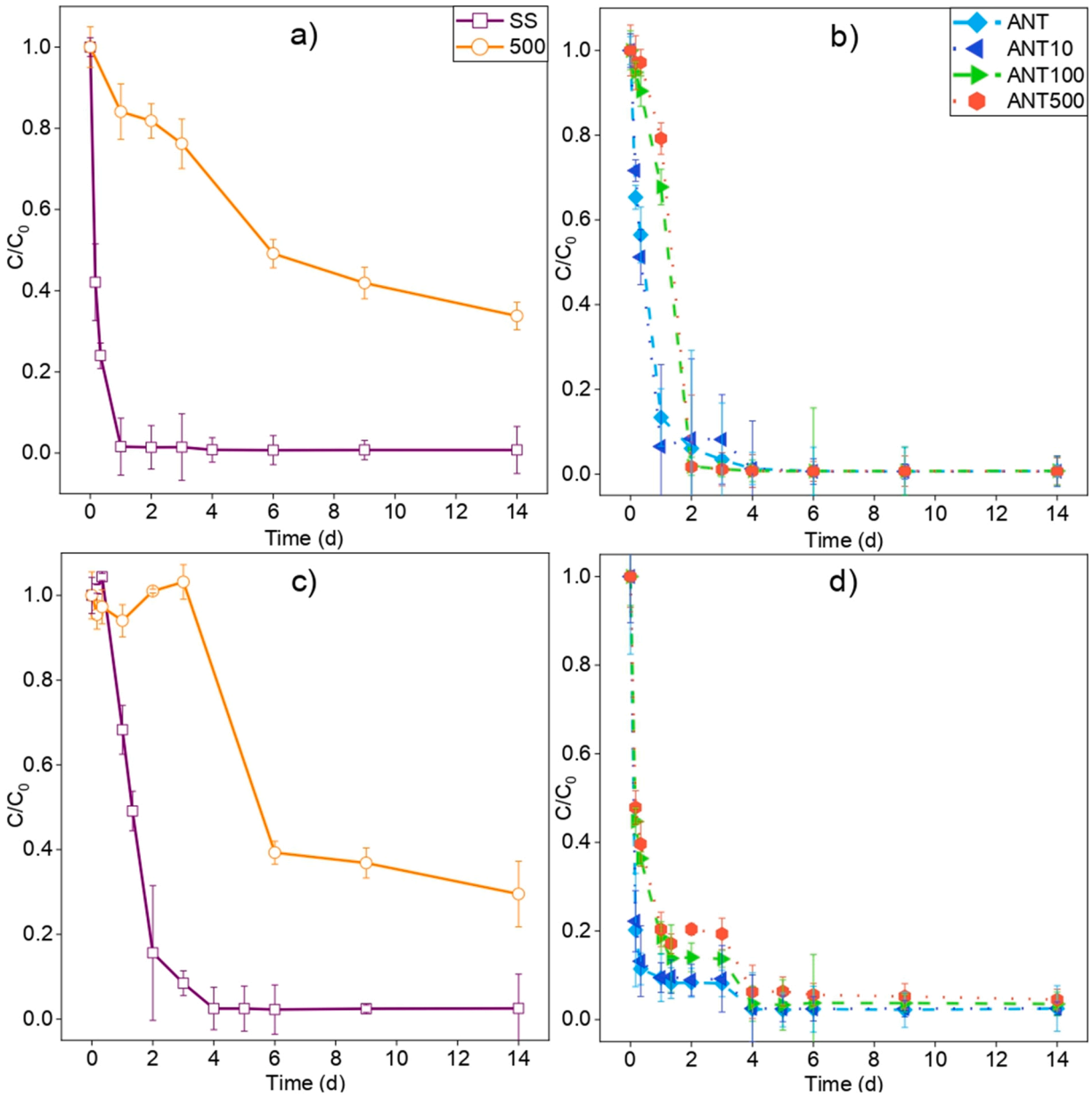

Fig. 6. Concentrations (C) of sulfamethoxazole (SMX) (**a**, **b**) and trimethoprim (TMP) (**c**, **d**) normalized to the initial value (C_0) measured in the experiments conducted with anaerobic sludge with 0, 10, 100, and 500 mg/L of GO added, sterilized sludge (SS) and 500 mg/L of GO (500). See Table 1 for details. The results are presented as mean values of triplicate measurements with standard deviations.

to biotransformation and not adsorption onto sludge, as explained further below. The decrease in TMP concentration with sterilized sludge (Fig. 6**c**) was similar to the biologically-active anaerobic sludge (5d) results, and TMP was entirely removed after three days. The gradual decrease in TMP concentration in the experiments with sterilized sludge also suggests biotransformation as the dominant removal mechanism, as adsorption would lead to a more abrupt decrease in concentration. Although autoclaving is considered as an efficient sludge sterilization technique, more so than for instance inhibition of sludge with sodium azide [47], this study indicated that the biological activity of the sludge was maintained resulting in biotransformation of both TMP and SMX, likely due to the presence of liberated intracellular enzymes that maintained their activity after autoclaving.

The concentration of TMP in the 500 mg/L GO solution remained unchanged in the first 3 days and then decreased to reach ~60% removal on day 6 of the experiment. SMX disappearance was more gradual in the presence of GO only, reaching around 65% removal by day 14. Both TMP and SMX can interact with graphene nanosheets of GO/RGO via π-π electron donor-acceptor interactions, electrostatic interactions, and hydrogen bonding [48–50]. TMP was present as uncharged species at an experimental pH of 7.2 (pK_a = 7.4, [51]) and strong π-π interactions were previously determined as the dominant adsorption mechanism of an uncharged TMP molecule at RGO nanosheets [50]. The decrease observed in the TMP adsorption onto GO between day 3 and 6 is likely a consequence of mild reduction and wrinkling of GO nanosheets at 35 °C, which was the temperature maintained in all experiments. Variations in the wrinkling of the graphene nanosheets can have a pronounced effect on the energy distribution of their adsorption sites and thus impact their interaction with SMX and TMP [49]. SMX was present as an anion (pK_{a1} = 1.4, pK_{a2} = 5.8, [52]), and may have been adsorbed more gradually to GO and partially reduced GO nanosheets due to the somewhat decreased π-π interactions, as GO has a negative charge within the range of pH 3–11 [53]. Previously, SMX adsorption in the GO dispersion was observed to

occur already within the first few hours [54,55].

In the experiments with biologically-active anaerobic sludge, SMX and TMP were rapidly removed in the first two days of the experiment and were not affected by the GO addition (**6b, 6d**). Similar results on rapid removal of SMX and TMP by mixed anaerobic communities were previously explained by the carbon-rich environment in the BMP assays, which facilitates their removal through co-metabolic degradation processes [55–57]. Thus, the presence of bioRGO did not further enhance the anaerobic biotransformation of the target antibiotics. However, the addition of GO had an impact on the amounts of the formed transformation products (TPs) of SMX.

For TMP, no TPs could be identified in any of the conducted experiments, including the target search for the previously reported products of TMP anaerobic transformation, e.g., formed by anaerobic demethylation [58]. Two TPs were identified for anaerobic degradation of SMX, including the protonated molecular ions, $[M+H]^+$ of 254 (TP253) and $[M+H]^+$ 258 (TP257). Product TP253 exhibited the identical MRM transitions as the parent compound (i.e., *m/z* 254→*m/z* 156.1, and *m/z* 254→*m/z* 92) but eluted at an earlier retention time (t_R) of 3.4 min compared with the t_R of SMX (5.5 min) (Fig. 7, Fig. S4). This, together with the identical mass spectra as compared to SMX (Fig. 7**a**), indicated a rearrangement in the isoxazole moiety in the SMX molecule to form TP253 (Fig. 7**b**). This rearrangement in TP253 was reported in a recent study on SMX transformation by sulfate-reducing and methanogenic communities [59]. In the same study, the authors observed another product with the nominal mass of 255 Da (molecular ion at *m/z* 256), formed by the cleavage of the N-O bond and isoxazole ring opening. Based on the obtained mass spectrum of TP257 (Fig. 7**c**), this product was likely formed via a similar pathway but involved further hydrogenation of the double bond in the isoxazole moiety. Such TPs are common

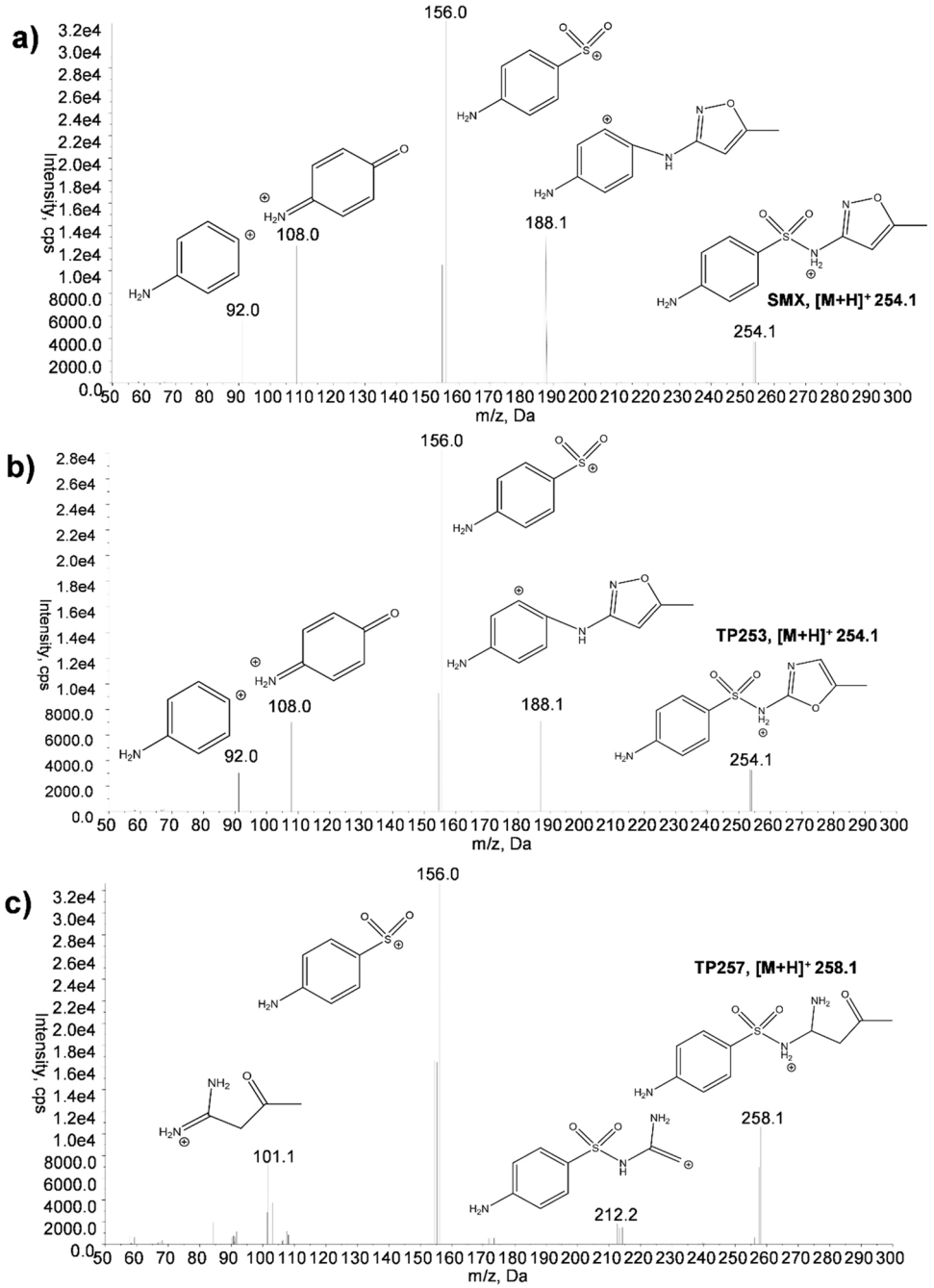

Fig. 7. Product ion spectra of **a)** sulfamethoxazole (SMX) and its transformation products (TPs): **b)** TP253, and **c)** TP257 and proposed fragment ion structures.

in anaerobic environments and are formed by sulfate-reducing bacteria and methanogenic cultures [59–61]. Thus, the anaerobic biotransformation of SMX proceeded via isomerization and N-O bond cleavage and reduction of the isoxazole moiety (Fig. S5), similar to previously reported data [59].

Although the addition of GO did not impact the SMX removal kinetics of the parent compound, it had a pronounced inhibiting impact on the formation of TP253 and TP257 (Fig. 8). For example, the amount of TP253 (estimated based on the peak area of the *m/z* 254 and normalized to the initial peak area of SMX) reached approximately 4% of the initial amount of SMX in the absence of GO, whereas the addition of 500 mg/L of GO lowered this value to a maximum of 1% (Fig. 8**a**). Similar behavior was observed for TP257, which reached 40% of the initial amount of SMX in the absence of GO, but only 16% in the presence of 500 mg/L of GO. The presence of 100 mg/L of GO gave similar results as in the case of AS without GO for both TP253 and TP257. This inhibiting effect of GO addition on the formation of TP253 and TP257 may have been a consequence of the consumption of the available electrons by the GO being the external electron acceptor. Yet the removal kinetics of the parent compound remained unchanged and the inhibiting effect of GO in the biotransformation of SMX could only be noted after its TPs were identified and their formation profiles determined. Furthermore, both TP253 and TP257 were also detected in the experiments conducted with the sterilized sludge. TP253 was rapidly formed and reached up to 12% of the initial amount of SMX within the first 24 h of the experiment, indicating that this compound was likely the primary biotransformation product of SMX. This result is surprising considering that viable sludge formed significantly lower quantities of TP253. Considering that the autoclaving treatment led to sludge lysis, it is likely that the formation of TP253 was enhanced by the liberation of specific intracellular enzymes. Intracellular enzymes were previously reported to play a significant role in the anaerobic biotransformation of antibiotics and other organic pollutants [62,63]. A recent study indicated a lower metabolic potential for the biotransformation of antibiotics via extracellular enzymes than via intracellular enzymes [62]. In the biotransformation of ciprofloxacin by the anaerobic sulfate-reducing bacteria, cytochrome P450 catalyzed hydroxylation and desethylation reaction in piperazinyl ring [63]. Nevertheless, it should be noted that denaturation of the cytochrome P450 enzyme is expected to occur at temperatures above 90ºC [64], and its contribution to the biotransformation of SMX, as well as the elucidation of key intracellular enzymes that were active in the sterilized sludge, require further study. From the qualitative profiles of TP253 and TP257 presented in Fig. 8, it can be observed that the appearance of new products does not occur simultaneously with the disappearance of the parent compound. Thus, anaerobic biotransformation of SMX likely included also other intermediate products that precede the formation of TP273 and TP257, and that could not be identified in the present study. The exception to this behavior is the experiment with the sterilized sludge, where a sharp decrease in SMX concentration is followed by a sharp increase in the amount of the formed TP253.

4. Conclusions and outlook

Rapid microbial reduction of GO to bioRGO occurred after one day of incubation with mixed anaerobic sludge. However, the formation of bioRGO negatively impacted the BMP (up to 21%) and did not influence the removal of selected antibiotics. Nevertheless, the addition of incremental amounts of GO led to a proportional decrease in the amounts of the identified biotransformation products of SMX, TP253 and TP257, formed via isomerization and N-O bond cleavage and reduction of the isoxazole moiety. Thus, although it was not evident from the removal kinetics of the parent compound, the anaerobic biotransformation of SMX was affected by the bioRGO presence. Furthermore, these products were measured in the sterilized sludge, indicating a prominent role of intracellular enzymes liberated upon the autoclaving in the anaerobic biotransformation of SMX. Thus, the results point out the necessity of a comprehensive evaluation of the impact of GO on the biotransformation of organic pollutants, including the analyses of their biotransformation products. Moreover, it is noted that BMP tests are not suitable to properly evaluate the impact of bioRGO on biogas production and organic micropollutants removal. Future studies should extend the investigation period to continuous systems.

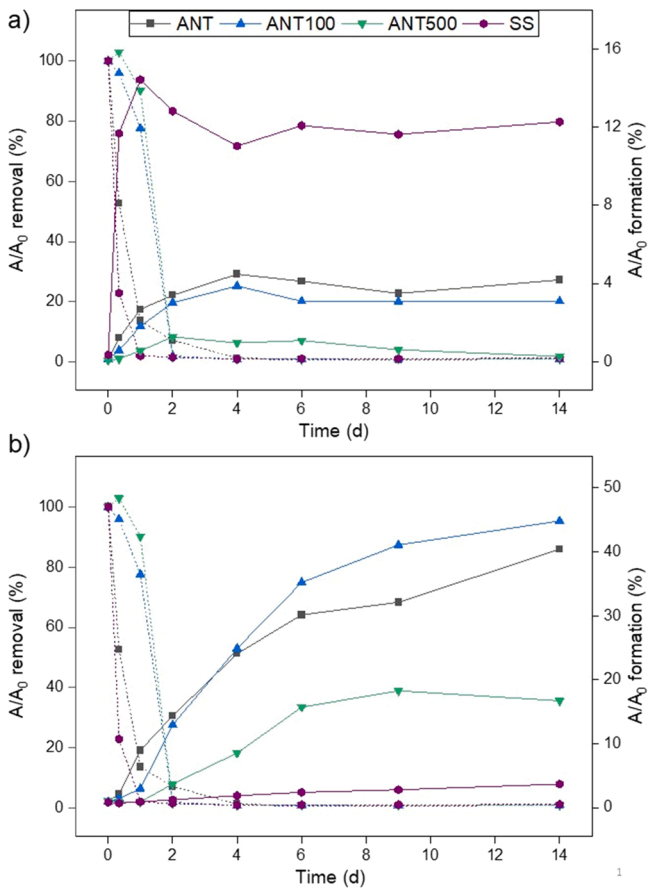

Fig. 8. Peak areas of: **a**) Transformation product 253 (TP253), and **b**) Transformation product 257 (TP257), obtained from the extracted ion chromatograms (XICs) and normalized to the initial value of peak area of sulfamethoxazole (SMX). Normalized concentrations of the parent compound (SMX) are presented in dotted lines for comparison. See Table 1 for details.

CRediT authorship contribution statement

Michele Ponzelli: Investigation, Data curation, Visualization, Formal analysis, Writing – original draft. **Soraya Zahedi:** Methodology, Writing – review & editing. **Konrad Koch:** Writing – review & editing, Supervision. **Jörg E. Drewes:** Writing – review & editing. **Jelena Radjenovic:** Conceptualization, Writing – review & editing, Supervision.

Declaration of Competing Interest

The authors declare that they have no known competing financial interests or personal relationships that could have appeared to influence the work reported in this paper.

Data availability

Data will be made available on request.

Acknowledgments

This work was supported by the European Union's Horizon 2020 research and innovation programme under the Marie Sklodowska-Curie grant agreement – MSCA-ITN-2018 (EJD Nowelties, grant number 812880). J.R. is grateful for the financial support provided by the Spanish State Research Agency of the Spanish Ministry of Science, Innovation, and Universities (PID2019-110346RB-C22), ANTARES Project.

Appendix A. Supporting information

Supplementary data associated with this article can be found in the online version at doi:10.1016/j.jece.2022.108373.

References

[1] D. Sedlak, Water 4.0: The past, present, and future of the world's most vital resource, Yale University (2014). https://doi.org/10.5860/choice.52–0292.
[2] W.W. Li, H.Q. Yu, B.E. Rittmann, Chemistry: reuse water pollutants, Nature 528 (2015) 29–31, https://doi.org/10.1038/528029a.
[3] P.L. McCarty, J. Bae, J. Kim, Domestic wastewater treatment as a net energy producer-can this be achieved? Environ. Sci. Technol. 45 (2011) 7100–7106, https://doi.org/10.1021/es2014264.
[4] L. Leng, P. Yang, S. Singh, H. Zhuang, L. Xu, W.H. Chen, J. Dolfing, D. Li, Y. Zhang, H. Zeng, W. Chu, P.H. Lee, A review on the bioenergetics of anaerobic microbial metabolism close to the thermodynamic limits and its implications for digestion applications, Bioresour. Technol. 247 (2018) 1095–1106, https://doi.org/10.1016/j.biortech.2017.09.103.
[5] C. Grandclément, I. Seyssiecq, A. Piram, P. Wong-Wah-Chung, G. Vanot, N. Tiliacos, N. Roche, P. Doumenq, From the conventional biological wastewater treatment to hybrid processes, the evaluation of organic micropollutant removal: a review, Water Res 111 (2017) 297–317, https://doi.org/10.1016/j.watres.2017.01.005.
[6] J. Zhang, W. Zhao, H. Zhang, Z. Wang, C. Fan, L. Zang, Recent achievements in enhancing anaerobic digestion with carbon- based functional materials, Bioresour. Technol. 266 (2018) 555–567, https://doi.org/10.1016/j.biortech.2018.07.076.
[7] Z. Chen, H. Li, W. Ma, D. Fu, K. Han, H. Wang, N. He, Q. Li, Y. Wang, Addition of graphene sheets enhances reductive dissolution of arsenic and iron from arsenic contaminated soil, Land Degrad. Dev. 29 (2018) 572–584, https://doi.org/10.1002/ldr.2892.
[8] N. Yoshida, Y. Miyata, K. Doi, Y. Goto, Y. Nagao, R. Tero, A. Hiraishi, Graphene oxide-dependent growth and self-Aggregation into a hydrogel complex of exoelectrogenic bacteria, Sci. Rep. 6 (2016) 21867, https://doi.org/10.1038/srep21867.
[9] L. Shen, Z. Jin, D. Wang, Y. Wang, Y. Lu, Enhance wastewater biological treatment through the bacteria induced graphene oxide hydrogel, Chemosphere 190 (2018) 201–210, https://doi.org/10.1016/j.chemosphere.2017.09.105.
[10] O. Akhavan, E. Ghaderi, Escherichia coli bacteria reduce graphene oxide to bactericidal graphene in a self-limiting manner, Carbon 50 (2012) 1853–1860, https://doi.org/10.1016/j.carbon.2011.12.035.
[11] G. Wang, F. Qian, C.W. Saltikov, Y. Jiao, Y. Li, Microbial reduction of graphene oxide by Shewanella, Nano Res 4 (2011) 563–570, https://doi.org/10.1007/s12274-011-0112-2.
[12] B. Virdis, P.G. Dennis, The nanostructure of microbially-reduced graphene oxide fosters thick and highly-performing electrochemically-active biofilms, J. Power Sources 356 (2017) 556–565, https://doi.org/10.1016/j.jpowsour.2017.02.086.
[13] D.R. Shaw, M. Ali, K.P. Katuri, J.A. Gralnick, L. Van Niftrik, M.S.M. Jetten, P. E. Saikaly, J. Reimann, R. Mesman, Extracellular electron transfer-dependent anaerobic oxidation of ammonium by anammox bacteria, Nat. Commun. 11 (2020) 2058, https://doi.org/10.1038/s41467-020-16016-y.
[14] B. Dong, Z. Xia, J. Sun, X. Dai, X. Chen, B.J. Ni, The inhibitory impacts of nano-graphene oxide on methane production from waste activated sludge in anaerobic digestion, Sci. Total Environ. 646 (2019) 1376–1384, https://doi.org/10.1016/j.scitotenv.2018.07.424.
[15] J. Zhang, Z. Wang, Y. Wang, H. Zhong, Q. Sui, C. Zhang, Y. Wei, Effects of graphene oxide on the performance, microbial community dynamics and antibiotic resistance genes reduction during anaerobic digestion of swine manure, Bioresour. Technol. 245 (2017) 850–859, https://doi.org/10.1016/j.biortech.2017.08.217.
[16] J.I. Bueno-López, C.H. Nguyen, J.R. Rangel-Mendez, R. Sierra-Alvarez, J.A. Field, F.J. Cervantes, Effects of graphene oxide and reduced graphene oxide on acetoclastic, hydrogenotrophic and methylotrophic methanogenesis, Biodegradation 31 (2020) 35–45, https://doi.org/10.1007/s10532-020-09892-0.
[17] T. Tian, S. Qiao, X. Li, M. Zhang, J. Zhou, Nano-graphene induced positive effects on methanogenesis in anaerobic digestion, Bioresour. Technol. 224 (2017) 41–47, https://doi.org/10.1016/j.biortech.2016.10.058.
[18] S. Liu, T.H. Zeng, M. Hofmann, E. Burcombe, J. Wei, R. Jiang, J. Kong, Y. Chen, Antibacterial activity of graphite, graphite oxide, graphene oxide, and reduced graphene oxide: Membrane and oxidative stress, ACS Nano 5 (2011) 6971–6980, https://doi.org/10.1021/nn202451x.
[19] Z. Guo, C. Xie, P. Zhang, J. Zhang, G. Wang, X. He, Y. Ma, B. Zhao, Z. Zhang, Toxicity and transformation of graphene oxide and reduced graphene oxide in bacteria biofilm, Sci. Total Environ. 580 (2017) 1300–1308, https://doi.org/10.1016/j.scitotenv.2016.12.093.
[20] F. Perreault, A.F. De Faria, S. Nejati, M. Elimelech, Antimicrobial properties of graphene oxide nanosheets: why size matters, ACS Nano 9 (2015) 7226–7236, https://doi.org/10.1021/acsnano.5b02067.
[21] A. Colunga, J.R. Rangel-Mendez, L.B. Celis, F.J. Cervantes, Graphene oxide as electron shuttle for increased redox conversion of contaminants under methanogenic and sulfate-reducing conditions, Bioresour. Technol. 175 (2015) 309–314, https://doi.org/10.1016/j.biortech.2014.10.101.
[22] L. Li, Q. Liu, Y.X. Wang, H.Q. Zhao, C.S. He, H.Y. Yang, L. Gong, Y. Mu, H.Q. Yu, Facilitated biological reduction of nitroaromatic compounds by reduced graphene oxide and the role of its surface characteristics, Sci. Rep. 6 (2016) 30082, https://doi.org/10.1038/srep30082.
[23] H. Fu, D. Zhu, Graphene oxide-facilitated reduction of nitrobenzene in sulfide-containing aqueous solutions, Environ. Sci. Technol. 47 (2013) 4204–4210, https://doi.org/10.1021/es304872k.
[24] E. Toral-Sánchez, J.R. Rangel-Mendez, J.A. Ascacio Valdés, C.N. Aguilar, F. J. Cervantes, Tailoring partially reduced graphene oxide as redox mediator for enhanced biotransformation of iopromide under methanogenic and sulfate-reducing conditions, Bioresour. Technol. 223 (2017) 269–276, https://doi.org/10.1016/j.biortech.2016.10.062.
[25] J.R.C. Team, J.R.C. Technical, Rep.: Sel. Subst. 3rd Watch List WFD (2020), https://doi.org/10.2760/194067.
[26] S. Aydin, B. Ince, Z. Cetecioglu, O. Arikan, E.G. Ozbayram, A. Shahi, O. Ince, Combined effect of erythromycin, tetracycline and sulfamethoxazole on performance of anaerobic sequencing batch reactors, Bioresour. Technol. 186 (2015) 207–214, https://doi.org/10.1016/j.biortech.2015.03.043.
[27] V. Mazzurco Miritana, G. Massini, A. Visca, P. Grenni, L. Patrolecco, F. Spataro, J. Rauseo, G.L. Garbini, A. Signorini, S. Rosa, A. Barra Caracciolo, Effects of sulfamethoxazole on the microbial community dynamics during the anaerobic digestion process, Front. Microbiol. 11 (2020) 1–12, https://doi.org/10.3389/fmicb.2020.537783.
[28] T. Tang, M. Liu, Y. Chen, Y. Du, J. Feng, H. Feng, Influence of sulfamethoxazole on anaerobic digestion: Methanogenesis, degradation mechanism and toxicity evolution, J. Hazard. Mater. 431 (2022), https://doi.org/10.1016/j.jhazmat.2022.128540.
[29] M. Gros, S. Rodríguez-Mozaz, D. Barceló, Rapid analysis of multiclass antibiotic residues and some of their metabolites in hospital, urban wastewater and river water by ultra-high-performance liquid chromatography coupled to quadrupole-linear ion trap tandem mass spectrometry, J. Chromatogr. A 1292 (2013) 173–188, https://doi.org/10.1016/j.chroma.2012.12.072.
[30] A. Göbel, A. Thomsen, C.S. McArdell, A.C. Alder, W. Giger, N. Theiß, D. Löffler, T. A. Ternes, Extraction and determination of sulfonamides, macrolides, and trimethoprim in sewage sludge, J. Chromatogr. A 1085 (2005) 179–189, https://doi.org/10.1016/j.chroma.2005.05.051.
[31] C. Holliger, M. Alves, D. Andrade, I. Angelidaki, S. Astals, U. Baier, C. Bougrier, P. Buffière, M. Carballa, V. De Wilde, F. Ebertseder, B. Fernández, E. Ficara, I. Fotidis, J.C. Frigon, H.F. De Laclos, D.S.M. Ghasimi, G. Hack, M. Hartel, J. Heerenklage, I.S. Horvath, P. Jenicek, K. Koch, J. Krautwald, J. Lizasoain, J. Liu, L. Mosberger, M. Nistor, H. Oechsner, J.V. Oliveira, M. Paterson, A. Pauss, S. Pommier, I. Porqueddu, F. Raposo, T. Ribeiro, F.R. Pfund, S. Strömberg, M. Torrijos, M. Van Eekert, J. Van Lier, H. Wedwitschka, I. Wierinck, Towards a standardization of biomethane potential tests, Water Sci. Technol. 74 (2016) 2515–2522, https://doi.org/10.2166/wst.2016.336.
[32] S.D. Hafner, S. Astals, P. Buffiere, N. Løjborg, C. Holliger, K. Koch, S. Weinrich, Calculation of Methane Production From From Manometric Measurements, Stand. BMP Methods Doc. 201, Version 2.6. (2020) Available online: ⟨https://www.dbfz.de/en/BMP. https://www.dbfz.de/en/BMP⟩.
[33] S.D. Hafner, S. Astals, C. Holliger, K. Koch, S. Weinrich, Calculation of Biochemical Methane Potential (BMP), Stand. BMP Methods Doc. 200, Version 1.6. (2020) Available online ⟨https://www.dbfz.de/en/BMP. https://www.dbfz.de/en/BMP⟩.
[34] R.B. Baird, A.D. Eaton, E.W. Rice, Standard Methods for the Examination of Water and Wastewater, 23rd ed., Washington, D.C., 2017.
[35] M.H. Zwietering, I. Jongenburger, F.M. Rombouts, K. Van't Riet, Modeling of the bacterial growth curve, Appl. Environ. Microbiol. 56 (1990) 1875–1881, https://doi.org/10.1128/aem.56.6.1875-1881.1990.
[36] S. Weinrich, M. Nelles, Basics of Anaerobic Digestion - Biochemical Conversion and Process Modelling, 2021. ⟨www.dnb.de⟩.
[37] S.D. Hafner, K. Koch, H. Carrere, S. Astals, S. Weinrich, C. Rennuit, Software for biogas research: tools for measurement and prediction of methane production, SoftwareX 7 (2018) 205–210, https://doi.org/10.1016/j.softx.2018.06.005.
[38] E.C. Salas, Z. Sun, A. Lüttge, J.M. Tour, Reduction of graphene oxide via bacterial respiration, ACS Nano 4 (2010) 4852–4856, https://doi.org/10.1021/nn101081t.
[39] S. Gurunathan, J.W. Han, V. Eppakayala, J.H. Kim, Microbial reduction of graphene oxide by Escherichia coli: a green chemistry approach, Colloids Surf. B Biointerfaces 102 (2013) 772–777, https://doi.org/10.1016/j.colsurfb.2012.09.011.
[40] Y. Lu, L. Zhong, L. Tang, H. Wang, Z. Yang, Q. Xie, H. Feng, M. Jia, C. Fan, Extracellular electron transfer leading to the biological mediated production of reduced graphene oxide, Chemosphere 256 (2020), 127141, https://doi.org/10.1016/j.chemosphere.2020.127141.
[41] K. Saravanan, G. Jayalakshmi, K. Suresh, B. Sundaravel, B.K. Panigrahi, D. M. Phase, Structural evaluation of reduced graphene oxide in graphene oxide during ion irradiation: X-ray absorption spectroscopy and in-situ sheet resistance

studies, Appl. Phys. Lett. 112 (2018), 111907, https://doi.org/10.1063/1.5025097.
[42] D. López-Díaz, M. López Holgado, J.L. García-Fierro, M.M. Velázquez, Evolution of the Raman spectrum with the chemical composition of graphene oxide, J. Phys. Chem. C. 121 (2017) 20489–20497, https://doi.org/10.1021/acs.jpcc.7b06236.
[43] Z. Lu, P. Girguis, P. Liang, H. Shi, G. Huang, L. Cai, L. Zhang, Biological capacitance studies of anodes in microbial fuel cells using electrochemical impedance spectroscopy, Bioprocess Biosyst. Eng. 38 (2015) 1325–1333, https://doi.org/10.1007/s00449-015-1373-z.
[44] K. Koch, S. Hafner, S. Astals, S. Weinrich, Evaluation of common supermarket products as positive controls in biochemical methane potential (BMP) tests, Water 12 (2020) 1223, https://doi.org/10.3390/w12051223.
[45] C. Holliger, H. Fruteau de Laclos, S.D. Hafner, K. Koch, S. Weinrich, S. Astals, M. Alves, D. Andrade, I. Angelidaki, L. Appels, S. Astals, S. Azman, E. Al., Requirements for measurement and validation of biochemical methane potential (BMP), Stand. BMP Methods Doc. 100, Version 1.3. (2020) Available online: ⟨https://www.dbfz.de/en/BMP. https://www.dbfz.de/en/BMP⟩.
[46] D. Wang, G. Wang, G. Zhang, X. Xu, F. Yang, Using graphene oxide to enhance the activity of anammox bacteria for nitrogen removal, Bioresour. Technol. 131 (2013) 527–530, https://doi.org/10.1016/j.biortech.2013.01.099.
[47] J.T. Trevors, Sterilization and inhibition of microbial activity in soil, J. Microbiol. Methods 26 (1996) 53–59, https://doi.org/10.1016/0167-7012(96)00843-3.
[48] F. Wang, S. Ma, Y. Si, L. Dong, X. Wang, J. Yao, H. Chen, Z. Yi, W. Yao, B. Xing, Interaction mechanisms of antibiotic sulfamethoxazole with various graphene-based materials and multiwall carbon nanotubes and the effect of humic acid in water, Carbon 114 (2017) 671–678, https://doi.org/10.1016/j.carbon.2016.12.080.
[49] S. Bai, X. Shen, G. Zhu, A. Yuan, J. Zhang, Z. Ji, D. Qiu, The influence of wrinkling in reduced graphene oxide on their adsorption and catalytic properties, Carbon 60 (2013) 157–168, https://doi.org/10.1016/j.carbon.2013.04.009.
[50] D.H. Carrales-Alvarado, I. Rodríguez-Ramos, R. Leyva-Ramos, E. Mendoza-Mendoza, D.E. Villela-Martínez, Effect of surface area and physical–chemical properties of graphite and graphene-based materials on their adsorption capacity towards metronidazole and trimethoprim antibiotics in aqueous solution, Chem. Eng. J. 402 (2020), 126155, https://doi.org/10.1016/j.cej.2020.126155.
[51] J. Aagaard, P.O. Madsen, P. Rhodes, T. Gasser, MICs of ciprofloxacin and trimethoprim for Escherichia coli: influence of pH, inoculum size and various body fluids, Infection 19 (1991) 167–169, https://doi.org/10.1007/BF01643691.
[52] A.L. Boreen, W.A. Arnold, K. McNeill, Photochemical fate of sulfa drugs in then aquatic environment: sulfa drugs containing five-membered heterocyclic groups, Environ. Sci. Technol. 38 (2004) 3933–3940, https://doi.org/10.1021/es0353053.
[53] S.W. Nam, C. Jung, H. Li, M. Yu, J.R.V. Flora, L.K. Boateng, N. Her, K.D. Zoh, Y. Yoon, Adsorption characteristics of diclofenac and sulfamethoxazole to graphene oxide in aqueous solution, Chemosphere 136 (2015) 20–26, https://doi.org/10.1016/j.chemosphere.2015.03.061.
[54] H. Chen, B. Gao, H. Li, Removal of sulfamethoxazole and ciprofloxacin from aqueous solutions by graphene oxide, J. Hazard. Mater. 282 (2015) 201–207, https://doi.org/10.1016/j.jhazmat.2014.03.063.
[55] R.B. Carneiro, L. Gonzalez-Gil, Y.A. Londoño, M. Zaiat, M. Carballa, J.M. Lema, Acidogenesis is a key step in the anaerobic biotransformation of organic micropollutants, J. Hazard. Mater. 389 (2020), 121888, https://doi.org/10.1016/j.jhazmat.2019.121888.
[56] L. Gonzalez-Gil, D. Krah, A.K. Ghattas, M. Carballa, A. Wick, L. Helmholz, J. M. Lema, T.A. Ternes, Biotransformation of organic micropollutants by anaerobic sludge enzymes, Water Res 152 (2019) 202–214, https://doi.org/10.1016/j.watres.2018.12.064.
[57] S. Wang, R. Yuan, H. Chen, F. Wang, B. Zhou, Anaerobic biodegradation of four sulfanilamide antibiotics: Kinetics, pathways and microbiological studies, J. Hazard. Mater. 416 (2021), 125840, https://doi.org/10.1016/j.jhazmat.2021.125840.
[58] B. Liang, D. Kong, M. Qi, H. Yun, Z. Li, K. Shi, E. Chen, A.S. Vangnai, A. Wang, Anaerobic biodegradation of trimethoprim with sulfate as an electron acceptor, Front. Environ. Sci. Eng. 13 (2019) 84, https://doi.org/10.1007/s11783-019-1168-6.
[59] W.Y. Ouyang, J. Birkigt, H.H. Richnow, L. Adrian, Anaerobic transformation and detoxification of sulfamethoxazole by sulfate-reducing enrichments and desulfovibrio vulgaris, Environ. Sci. Technol. 55 (2021) 271–282, https://doi.org/10.1021/acs.est.0c03407.
[60] Y. Jia, S.K. Khanal, H. Zhang, G.H. Chen, H. Lu, Sulfamethoxazole degradation in anaerobic sulfate-reducing bacteria sludge system, Water Res 119 (2017) 12–20, https://doi.org/10.1016/j.watres.2017.04.040.
[61] T. Alvarino, P. Nastold, S. Suarez, F. Omil, P.F.X. Corvini, H. Bouju, Role of biotransformation, sorption and mineralization of 14C-labelled sulfamethoxazole under different redox conditions, Sci. Total Environ. 542 (2016) 706–715, https://doi.org/10.1016/j.scitotenv.2015.10.140.
[62] M.T. Zumstein, D.E. Helbling, Biotransformation of antibiotics: exploring the activity of extracellular and intracellular enzymes derived from wastewater microbial communities, Water Res 155 (2019) 115–123, https://doi.org/10.1016/j.watres.2019.02.024.
[63] Y. Jia, S.K. Khanal, H. Shu, H. Zhang, G.H. Chen, H. Lu, Ciprofloxacin degradation in anaerobic sulfate-reducing bacteria (SRB) sludge system: Mechanism and pathways, Water Res 136 (2018) 64–74, https://doi.org/10.1016/j.watres.2018.02.057.
[64] S.A. Maves, Understanding thermostability in cytochrome P450 by combinatorial mutagenesis, Protein Sci. 10 (2001) 161–168, https://doi.org/10.1110/ps.17601.